Inorg. Chem. **2005**, *44*, 6879–6892

Forum

Molecular Chemistry of Consequence to Renewable Energy

Jillian L. Dempsey, Arthur J. Esswein, David R. Manke, Joel Rosenthal, Jake D. Soper, and Daniel G. Nocera*

Department of Chemistry, 6-335, Massachusetts Institute of Technology, 77 Massachusetts Avenue, Cambridge, Massachusetts 02139-4307

Received June 8, 2005

Energy conversion cycles are aimed at driving unfavorable, small-molecule activation reactions with a photon harnessed directly by a transition-metal catalyst or indirectly by a transition-metal catalyst at the surface of a photovoltaic cell. The construction of such cycles confronts daunting challenges because they rely on chemical transformations not understood at the most basic levels. These transformations include multielectron transfer, proton-coupled electron transfer, and bond-breaking and -making reactions of energy-poor substrates. We have begun to explore these poorly understood areas of molecular science with transition-metal complexes that promote hydrogen production and oxygen bond-breaking and -making chemistry of consequence to water splitting.

1. Introduction

A great technological challenge facing our global future is the development of renewable energy. Rising standards of living in a growing world population will cause global energy consumption to increase dramatically over the next half century. Energy consumption is predicted to increase at least twofold, from our current burn rate of 12.8 TW to 28−35 TW by 2050.[1,2] A short-term response to this challenge is the use of methane and other petroleum-based fuels as hydrogen sources.[3] However, external factors of economy, environment, and security dictate that this energy need be met by renewable and sustainable sources[3−9] with water emerging prominently as the primary carbon-neutral hydrogen source and light as an energy input. A response to this "grand challenge" of chemistry, however, faces a daunting hurdle: large expanses of *fundamental molecular science* await discovery if the sun and water are to be used as an energy source.

Unexplored basic science issues are immediately confronted when the water-splitting problem is posed in the simplest chemistry framework:

$$2H_2O \xrightarrow[PC]{h\nu} 2H_2 + O_2$$

$$4H^+ + 4e^- \rightarrow 2H_2$$

$$2H_2O \rightarrow O_2 + 4H^+ + 4e^-$$

The overall transformation is a *multielectron* process. The treatment of even a single-electron reaction represents such

* To whom correspondence should be addressed. E-mail: nocera@mit.edu.

(1) Hoffert, M. I.; Caldeira, K.; Jain, A. K.; Haites, E. F.; Harvey, L. D. D.; Potter, S. D.; Schlesinger, M. E.; Schneider, S. H.; Watts, R. G.; Wigley, T. M. L.; Wuebbles, D. J. *Nature* **1998**, *395*, 881−884.
(2) Lewis, N. S. *Energy and Transportation*; The National Academies Press: Washington, DC, 2003; pp 33−39.
(3) *Basic Research Needs for the Hydrogen Economy*; A Report from the Basic Energy Sciences Workshop on Hydrogen Production, Storage, and Use; U.S. Department of Energy: Washington, DC, 2003.
(4) *World Energy Assessment Report: Energy and the Challenge of Sustainability*; United Nations Development Program; United Nations: New York, 2003.
(5) *Basic Research Needs to Assure a Secure Energy Future*; A Report from the Basic Energy Sciences Advisory Committee; U.S. Department of Energy: Washington, DC, 2003.
(6) Karas, T. H. *Energy and National Security*; Sandia Report SAND2003-3287; Sandia National Laboratories: Albuquerque, NM, 2003.
(7) Address to the National Hydrogen Association, Secretary of Energy Spencer Abraham, Mar 5, 2003; available at http://www.energy.gov/engine/content.do?PUBLIC_ID=13384&BT_CODE=PR_SPEECHES&TT_CODE=PRESSRELEASE.
(8) The Effect on the National Security of Imports of Crude Oil and Refined Petroleum Products; U.S. Department of Commerce, An Investigation Conducted Under Section 232 of the Trade Expansion Act of 1962, as Amended, Nov 1999; p ES-9.
(9) Goodstein, D. *Out of Gas: The End of the Age of Oil*; Norton: New York, 2004.

10.1021/ic0509276 CCC: $30.25
Published on Web 09/26/2005

an important milestone of chemistry that it was worthy of Nobel Prizes.[10,11] A similar understanding about multielectron redox reactions has yet to be realized. Moreover, proton transfer must accompany electron transfer [i.e., proton-coupled electron transfer (PCET)]:[12] both *electron and proton inventories* need to be managed.[13] Also, if these challenges were not enough, water splitting confronts sizable thermodynamic and kinetic barriers that must be overcome, thus bringing another set of unexplored frontiers to the table. Over the past 3 decades, practitioners at the forefront of chemistry have catalytically made and broken energy-rich bonds in downhill reactions. However, efficient *bond-making/breaking reactions on energy-poor substrates* have yet to be realized at a molecular center or at a surface. This is especially pertinent to the water-splitting problem because the byproduct of water activation at the photocatalyst (PC), whether molecule or solid, will invariably yield species with strong metal−oxygen bonds. These bonds need to be *activated* to close a catalytic cycle.

The photochemical water-splitting problem shares basic chemical commonalities to the activation of other small molecules of energy consequence as well, including CO_2, N_2, CH_4, H_2, and O_2. All involve *bond-making and -breaking* processes that require *multielectron* transfers often coupled to *proton-transfer* events. Our research efforts have addressed the foregoing italicized research themes by expanding the reactivity of metal complexes in ground and electronic excited states beyond conventional one-electron transfer and by developing new experimental methods that permit multielectron, PCET, and atom-transfer reactions to be examined at a mechanistic level. Our recent contributions in these areas are summarized below with the inclusion of recent research results in the area of dinuclear gold chemistry.

2. Hydrogen Photoproduction

2.1. Two-Electron Mixed-Valence Complexes. We have exploited two-electron mixed valency in managing the multielectron chemistry of hydrogen activation and production. The motivation for developing this line of research is straightforward: as single-electron mixed-valence ($M^n\cdots M^{n+1}$) compounds react in one-electron steps,[14,15] two-electron mixed-valence ($M^n\cdots M^{n+2}$) compounds can react in two-electron steps at the constituent redox sites, regardless of whether they are metal- or ligand-based. This approach does not necessarily demand that each metal reacts in a concerted two-electron step. Rather, it requires that the typical single-electron redox products be kinetically and/or thermodynamically unstable with respect to the two-electron redox products. In this manner, even if the primary photoevent

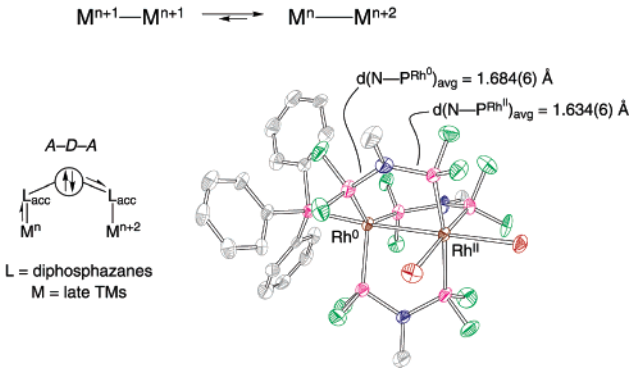

Figure 1. (Top) Internal disproportionation reaction of a bimetallic core that needs to be exploited for the establishment of two-electron mixed valency. (Bottom, left) Three-atom bridging ligand possessing an electron donor bridge (D) between two π-accepting moieties (A), which can be used to stabilize two-electron mixed-valence cores. The diphosphazane ligands shown in Scheme 1 incorporate this A−D−A stereoelectronic motif. The stabilization of a mixed-valence core results in differing bond orders indicative of an asymmetric electronic distribution. (Bottom, right) Crystal structure of $Rh_2^{0,II}(dfpma)_3Br_2$ displaying the long−short bond alteration of the ligand backbone.

Scheme 1

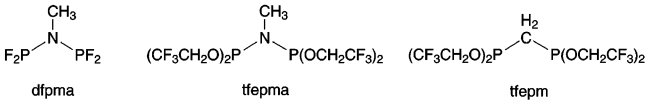

involves single-electron transfer, an ensuing redox event will be facile, thus driving net multielectron reactivity.

The issue of two-electron mixed valency is controlled by the electronic properties of the coordinating ligand. As shown in Figure 1, the two-electron mixed-valence state is attained by the disproportionation of a redox symmetric core. To accomplish this task, we have explored the two limiting ligand-design approaches: two π-accepting moieties with a π-donor bridge (A−D−A)[16−20] and the antithetical, two π-donating moieties with a π-accepting bridge (D−A−D).[21−23] The stabilization of metals that differ by two in their formal oxidation state is indicated by the arrows in Figure 1. We have found the A−D−A motif to exhibit a particular proclivity for stabilizing formal $M^n\cdots M^{n+2}$ cores. Three ligands that have been useful to the studies described here are shown in Scheme 1. The bis(difluorophosphino)methylamine (dfpma, $CH_3N(PF_2)_2$) and bis[bis(trifluoroethoxy)phosphino]methylamine (tfepma, $CH_3N[P(OCH_2CF_3)_2]_2$) ligands incorporate an A−D−A motif by placing an amine bridge between two electron-deficient phosphines (PR^F_2) or phosphites ($P(OR^F)_2$); in the bis[bis(trifluoroethoxy)phosphino]methane (tfepm, $CH_2[P(OCH_2CF_3)_2]_2$) ligand, the amine donor bridge is replaced by a methylene unit. The

(10) Marcus, R. A. *Angew. Chem., Int. Ed. Engl.* **1993**, *32*, 1111−1121.
(11) Taube, H. *Angew. Chem., Int. Ed. Engl.* **1984**, *23*, 329−339.
(12) Cukier, R. I.; Nocera, D. G. *Annu. Rev. Phys. Chem.* **1998**, *49*, 337−369.
(13) Chang, C. J.; Chang, M. C. Y.; Damrauer, N. H.; Nocera, D. G. *Biophys. Biochim. Acta* **2004**, *1655*, 13−28.
(14) Vogler, A.; Osman, A. H.; Kunkely, H. *Coord. Chem. Rev.* **1985**, *64*, 159−173.
(15) Meyer, T. J. *Prog. Inorg. Chem.* **1983**, *30*, 389−440.
(16) Heyduk, A. F.; Macintosh, A. M.; Nocera, D. G. *J. Am. Chem. Soc.* **1999**, *121*, 5023−5032.
(17) Odom, A. L.; Heyduk, A. F.; Nocera, D. G. *Inorg. Chim. Acta* **2000**, *297*, 330−337.
(18) Heyduk, A. F.; Nocera, D. G. *J. Am. Chem. Soc.* **2000**, *122*, 9415−9426.
(19) Heyduk, A. F.; Nocera, D. G. *Chem. Commun.* **1999**, 1519−1520.
(20) Veige, A. S.; Nocera, D. G. *Chem. Commun.* **2004**, 1958−1959.
(21) Manke, D. R.; Nocera, D. G. *Inorg. Chim. Acta* **2003**, *345*, 235−240.
(22) Manke, D. R.; Nocera, D. G. *Inorg. Chem.* **2003**, *42*, 4431−4436.
(23) Manke, D. R.; Loh, Z.-H.; Nocera, D. G. *Inorg. Chem.* **2004**, *43*, 3618−3624.

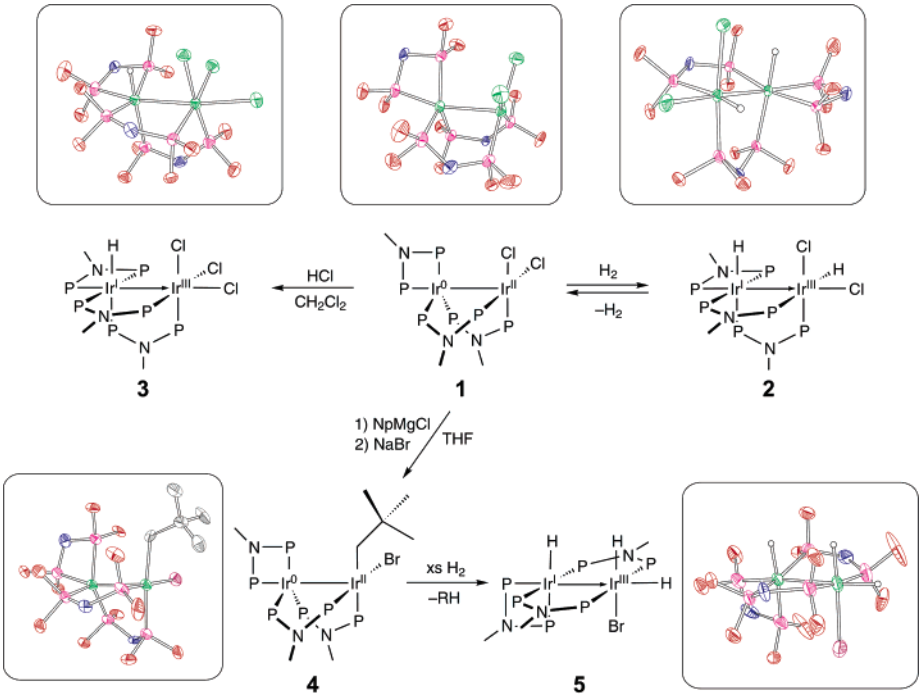

Figure 2. Hydride and hydrido−halo chemistry of two-electron mixed-valence diiridium complexes. Thermal ellipsoids are drawn at the 50% probability level, and the N−Me and $-CH_2CF_3$ groups of the tfepma ligand have been omitted for clarity.

dfpma and tfepma diphosphazane ligands are particularly useful for driving the internal disproportionation of binuclear $M_2^{I,I}$ cores to $M_2^{0,II}$ cores[24] for the metals rhodium[16,17] and iridium.[18−20] X-ray crystal structures reveal a pronounced asymmetry in the diphosphazane framework upon ligation to a bimetallic core.[16] The result is consistent with asymmetric π donation of the amine bridge lone pair to the PR^F_2 bonded to M^{II}. With $M^{II} \rightarrow PR^F_2$ π back-bonding diminished, the PR^F_2 group acts more like a simple σ donor, stabilizing the high-valent M^{II} metal center. Correspondingly, with the nitrogen lone pair electron density channeled away from the second neighboring PR^F_2 group, its strong π-accepting properties are maintained, and hence M^0 is stabilized. As shown in Figure 1, this electronic asymmetry is reflected in an alternating bond length pattern for the Rh^0−P−N−P−Rh^{II} framework.

The benefit of designing authentic two-electron mixed-valence complexes is the ability to effect multielectron redox chemistry among discrete molecular species. With the metals working in concert, two- and four-electron transformations are promoted along ground- and excited-state pathways.[16−18,20] Reactivity pertinent to hydrogen management and photoproduction at M^n−M^{n+2} cores is now described.

2.2. Hydrogen Management at Two-Electron Mixed-Valence Cores. The role of two-electron mixed valency in hydrogen activation was examined using diiridium species because the increased stability of third-row M−H bonds facilitates the isolation and study of such metal hydrido complexes, as evidenced by the results shown in Figure 2. Experimental and computational studies of these diiridium complexes provide a consistent picture for H_2 reactivity at M^n−M^{n+2} cores.[25] Addition of H_2 to a M^0−$M^{II}(X)_2$ occurs at the M^{II} end of the bimetallic core, and addition is mediated by a bridging hydride. For addition to the Ir^0−$Ir^{II}(X)_2$ cores of **1**, the bridging hydride must come from the reactant; a halogen must swing from the equatorial position to allow the entering hydrogen atom to access the bridge position:

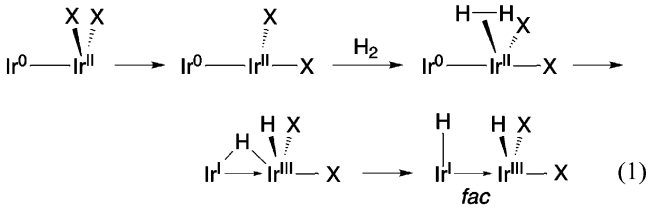

(1)

As shown by eq 1, this H_2 addition pathway leads to the *fac* stereochemistry observed in Figure 2 for the addition of H_2 and HCl to **1**, yielding **2** and **3**, respectively. A similar μ-H intermediate prevails for hydrogen atom migration at Ir^0−$Ir^{II}(H)(X)$ cores,[26] which may be generated by the addition of H_2 to **4** (Figure 2). The terminal hydride (H_a in eq 2) that is present from the outset may smoothly fold over into the bridging position as hydrogen attacks the axial coordination site to give product **5** (Figure 2) with *mer* stereochemistry about the Ir^{III} center.

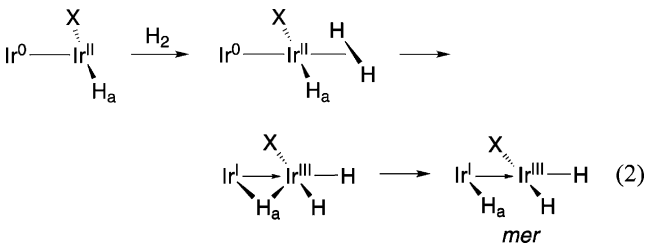

(2)

(24) Gray, T. G.; Nocera, D. G. *Chem. Commun.* **2005**, 1540−1542.

Scheme 2

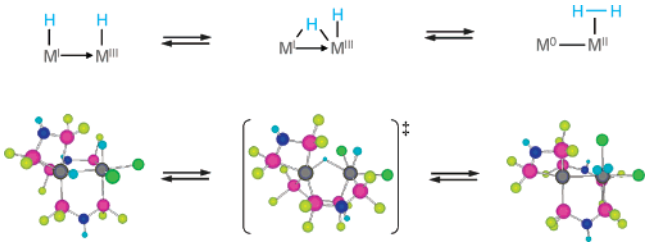

In this case, the hydrogen atom is able to traverse the diiridium core without the need for swinging a terminal ligand from an equatorial site.

The microscopic reverse of the H_2 addition process is reductive elimination, and accordingly the bridging hydride is expected to be a critical intermediate for H_2 evolution. The results presented in Scheme 2 support this contention. A critical determinant for the reactivity of H_2 at M^n-M^{n+2} cores appears to be the ability to establish intermetal redox cooperation for hydrogen atom migration. As argued by Bosnich,[27,28] low-energy ligand flexing modes are important requisites to cooperative reactivity between metal centers. For H_2 reactivity at $M^n\cdots M^{n+2}$ dimers, the diphosphazane ligand accommodates the disparate coordination geometries of the metal centers during the course of the hydrogen atom migration.

Hydrogen addition and elimination via a bridging hydride transition state is akin to bimolecular binuclear elimination pathways.[26] Some metal hydrides, which exhibit sluggish intramolecular elimination, are known to be extremely unstable in the presence of a second complex capable of attaining coordinative unsaturation. This enhanced reactivity has been ascribed to the following transformation,[29−31]

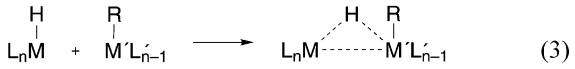

(3)

in which R is a hydride, alkyl, or acyl. Dinuclear elimination of this type is only possible when at least one of the ligands is a hydride, which must migrate to the bridging position for elimination to occur. For the case of the mixed-valence compounds, the coordinative unsaturation and hydride are already present. With the neighboring metals of a $M^n\cdots M^{n+2}$ core working in concert, the hydrogen atom migrates to and from the critical bridging position to promote facile H_2 addition and elimination,[25] respectively.

2.3. Hydrido−Halide Photochemistry of Two-Electron Mixed-Valence Cores of Dirhodium. Hydrogen elimination becomes facile when the metal−hydride bond is weakened by moving to a bimetallic core composed of the second-row metal rhodium. By the incorporation of a dσ^* excited state within the electronic structure of dirhodium dfpma complexes,[32−35] the cycle shown in Figure 3 may be constructed for the photoproduction of hydrogen from homogeneous solutions.[36] In brief, a photon removes an axial CO from the $Rh_2^{0,0}$ complex, opening a coordination site for HX attack (the axial site may also be opened thermally). Disappearance of the $Rh_2^{0,0}$ complex is accompanied by the formation of 1 equiv of H_2, and the appearance of a blue intermediate, which quickly converts to the $Rh^0-Rh^{II}X_2$ complex. The $Rh^{II}-X$ bond may be photoactivated in the presence of a halogen trap, thus closing the photocycle. In this phototransformation, H_2 elimination is facile and neither hydride− nor hydrido−halide intermediates are observed.

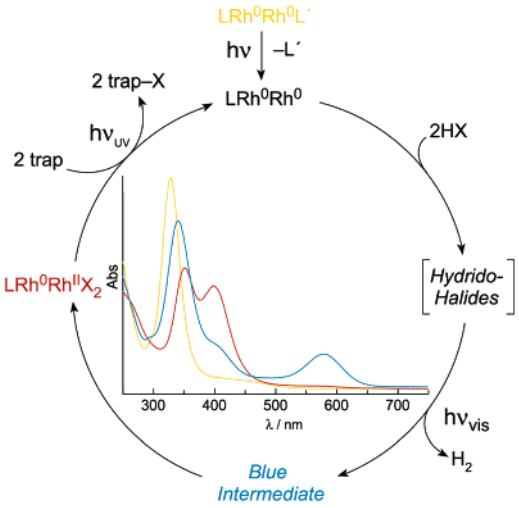

Figure 3. Photocycle for H_2 production from homogeneous HX solutions with a two-electron mixed-valence $Rh_2^{0,II}$ core as the key intermediate for Rh−X photoactivation. Only the formal oxidation states of the dirhodium core are shown; the bimetallic center is strapped by three dfpma ligands.

Models of the intermediates of the photocycle may be revealed by tuning the electronic structure of the bridging ligand. Figure 4 emphasizes the relation between the bridging ligand's electronic structure and the formal oxidation state of the binuclear core. The A−D−A motif (vide supra) stabilizes $M^n\cdots M^{n+2}$ cores. Conversely, the typical chemistry of dirhodium[37−42] shows that a valence-symmetric bimetallic core is obtained for "electronically neutral" ligands such as bridging phosphines. By tuning of the donating properties of the bridgehead and the electron-withdrawing properties of the phosphine, the formal oxidation state of the bimetallic

(25) Gray, T. G.; Veige, A. S.; Nocera, D. G. *J. Am. Chem. Soc.* **2004**, *126*, 9760−9768.
(26) Veige, A. S.; Gray, T. G.; Nocera, D. G. *Inorg. Chem.* **2005**, *44*, 17−26.
(27) Bosnich, B. *Inorg. Chem.* **1999**, *38*, 2554−2562.
(28) McCollum, D. G.; Bosnich, B. *Inorg. Chim. Acta* **1998**, *270*, 13−19.
(29) Norton, J. R. *Acc. Chem. Res.* **1979**, *12*, 139−145.
(30) Martin, B. D.; Warner, K. E.; Norton, J. E. *J. Am. Chem. Soc.* **1986**, *108*, 33−39.
(31) Kristjánsdóttir, S. S.; Norton, J. A. In *Transition Metal Hydrides*; Dedieu, A., Ed.; VCH: New York, 1992; Chapter 9, pp 309−360.
(32) Kadis, J.; Shin, Y.-g. K.; Dulebohn, J. I.; Ward, D. L.; Nocera, D. G. *Inorg. Chem.* **1996**, *35*, 811−817.
(33) Heyduk, A. F.; Krodel, D. J.; Meyer, E. E.; Nocera, D. G. *Inorg. Chem.* **2002**, *41*, 634−636.
(34) Dulebohn, J. I.; Ward, D. L.; Nocera, D. G. *J. Am. Chem. Soc.* **1990**, *112*, 2969−2977.
(35) Dulebohn, J. I.; Nocera, D. G. *J. Am. Chem. Soc.* **1988**, *110*, 4054−4056.
(36) Heyduk, A. F.; Nocera, D. G. *Science* **2001**, *293*, 1639−1641.
(37) Mague, J. T.; Mitchener, J. P. *Inorg. Chem.* **1969**, *8*, 119−125.
(38) Sanger, A. R. *J. Chem. Soc., Chem. Commun.* **1975**, 893−894.
(39) Balch, A. L.; Tulyathan, B. *Inorg. Chem.* **1977**, *16*, 2840−2845.
(40) Kubiak, C. P.; Eisenberg, R. *J. Am. Chem. Soc.* **1977**, *99*, 6129−6131.
(41) Cowie, M.; Mague, J. T.; Sanger, R. A. *J. Am. Chem. Soc.* **1978**, *100*, 3628−3629.
(42) Balch, A. L. *J. Am. Chem. Soc.* **1976**, *98*, 8049−8054.

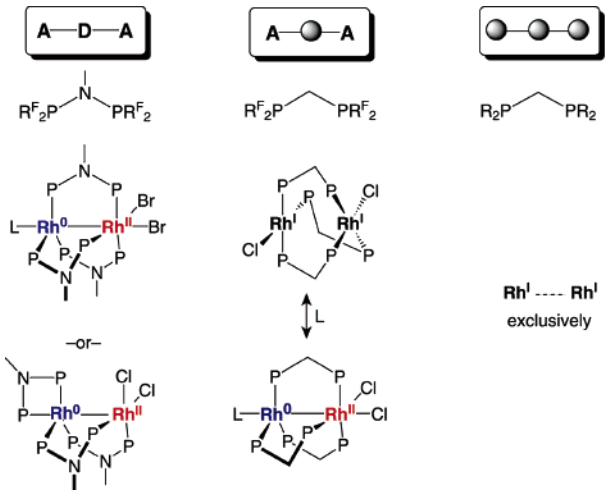

Figure 4. Schematic demonstrating the relation of the electronic structure of a bridging bidentate ligand on the formal oxidation state of a dirhodium binuclear core.

core can be adjusted between valence symmetry and asymmetry (middle panel), thus allowing us to unveil the relevant intermediates of the photocycle shown in Figure 3.

The proposed dihydride products of HX addition to a dirhodium core are obtained when the electronic accepting properties of the ligand are changed from $-PF_2$ of dfpma to the slightly less accepting and more bulky $-P(OCH_2CF_3)_2$ groups of tfepma. We have synthesized and isolated the three dihydride isomers of Figure 5. These compounds are models of the primary products of HX addition to the $Rh_2^{0,0}$ core. The syn isomer, **6**, slowly (~24 h) converts to **7** and **8**, which conversely interconvert rapidly on the NMR time scale. Because conversion of **6** to **7** and **8** is slow, its photochemistry may be examined without the complicating participation of the other isomers.

Photolysis of **6** promptly yields 1 equiv of H_2, as determined by Toepler pump measurements, and a compound with an absorption profile that is nearly identical with that of the elusive blue compound of Figure 3. Photolyzed solutions of **6** and **6**-d_2 give only H_2 and D_2, respectively, indicating that H_2 photoelimination proceeds via an intramolecular pathway. We suspect that the elimination proceeds via the bridging hydride intermediate discussed in section 2.2. We have independently prepared and isolated a blue-purple compound by replacing the N−Me bridgehead of tfepma with the methylene unit of tfepm, $H_2C[P(OCH_2CF_3)_2]_2$. An X-ray crystal structure of the compound shows it to be the $Rh_2^{I,I}(Cl)_2$ complex, **9** (Figure 5), where three phosphite ligands and a chloride assume the approximately square-planar geometry of a face-to-face $d^8\cdots d^8$ bimetallic complex. Spectroscopic experiments establish that the low-energy absorption band is due to a $d\sigma^* \rightarrow p\sigma$ transition, which is the signature transition of face-to-face $d^8\cdots d^8$ transition-metal complexes.[42−44] We have also prepared the $d^8\cdots d^8$ dimer of iridium, **10** (Figure 5). In this case, we are on the razor's edge of mixed valency as symmetric **10** converts to **11**, the structure of which is shown in Figure 5. Compound **11** is a fascinating complex with a chloride ion folded over into a bridging position. The compound is a snapshot of the intermetal chloride migration that takes the symmetric $(Cl)M^I\cdots M^I(Cl)$ core to an internally disproportionated $M^0-M^{II}(Cl)_2$ core; its existence also highlights the proclivity of phosphorus−nitrogen−phosphorus (PNP) ligand systems (dfpma and tfepma) to stabilize asymmetric two-electron mixed-valence cores.

Based on the chemistry of tfepma and tfepm dirhodium analogues, we propose that the dirhodium dfpma photocatalyst produces H_2 from HX by the photocycle shown in Figure 6. HX addition to the $Rh_2^{0,0}$ core produces the $Rh_2^{II,II}$ dihydride−dihalide, which photoeliminates 1 equiv of H_2 and generates the blue $(X)Rh^I\cdots Rh^I(X)$ complex. This valence-symmetric, primary photoproduct is unstable with respect to internal disproportionation to $Rh^0-Rh^{II}(X)_2$; the disproportionation proceeds by folding a terminal halide into the bridging position of the dirhodium core. Photoexcitation of $Rh^0-Rh^{II}(X)_2$ leads to halogen elimination and regeneration of the Rh^0Rh^0 complex, for re-entry into the photocycle.

The overall photoefficiency for H_2 production is ~1%. This photoefficiency is the same as that measured independently for the photoconversion of $Rh_2^{0,II}(dfpma)_3Cl_2L$ to $Rh_2^{0,0}(dfpma)_3L_2$ ($\phi_p = 7 \times 10^{-3}$). Together these results indicate that the activation of the Rh−X bond is determinant to the overall photocatalytic activity. An increase in the quantum efficiency for hydrogen photocatalysis is, therefore, equated to increasing the photoefficiency for halogen elimination from the binuclear metal core. Toward this end, we have begun to explore alternative strategies for the multielectron photoactivation of M−X bonds. We were initially attracted to porphyrins of high-valent and early transition metals because (1) the *cis*-halide arrangement of early-transition-metal porphyrins[45−47] might be conducive to X−X coupling and (2) metalloporphyrin systems may be expected to react smoothly with HX to produce hydrogen and the metal dihalide based on the results of early-transition-metal cyclopentadienyl complexes,[48,49] which are surrogates of group IV metalloporphyrins. However, we discovered that photoexcitation of *cis*-dihalide metalloporphyrins results in photoreduction of the porphyrin macrocycle, thereby circumventing M−X photoactivation.[50] We have also explored the prospects of using ligand-based two-electron mixed valency of porphyrinogens.[51,52] The goal here is to use the macrocycle to provide the multielectron equivalents needed for M−X activation. Most recently, we have turned our attention to using the more oxidizing bimetallic centers of

(43) Rice, S. F.; Gray, H. B. *J. Am. Chem. Soc.* **1981**, *103*, 1593−1595.
(44) Fordyce, W. A.; Brummer, J. G.; Crosby, G. A. *J. Am. Chem. Soc.* **1981**, *103*, 7061−7064.
(45) Brand, H.; Arnold, J. *J. Am. Chem. Soc.* **1992**, *114*, 2266−2267.
(46) Kim, H.-J.; Whang, D.; Kim, K.; Do, Y. *Inorg. Chem.* **1993**, *32*, 360−362.
(47) Brand, H.; Arnold, J. *Organometallics* **1993**, *12*, 3655−3665.
(48) Shibata, K.; Aida, T.; Inoue, S. *Chem. Lett.* **1992**, 1171−1176.
(49) Wailes, P. C.; Weigold, H. *J. Organomet. Chem.* **1970**, *2*, 405−411.
(50) Pistorio, B. J.; Nocera, D. G. *J. Photochem. Photobiol. A* **2004**, *162*, 563−567.
(51) Bachmann, J.; Nocera, D. G. *J. Am. Chem. Soc.* **2004**, *126*, 2829−2837.
(52) Bachmann, J.; Nocera, D. G. *J. Am. Chem. Soc.* **2005**, *127*, 4730−4743.

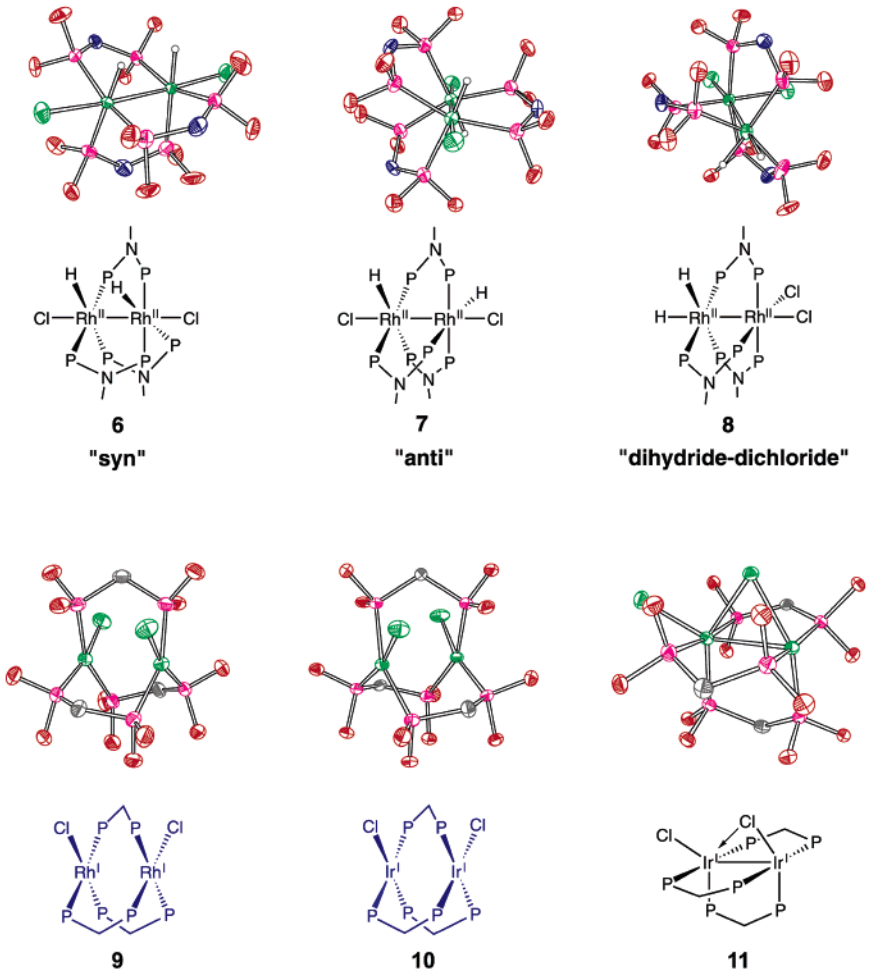

Figure 5. Model compounds relevant to the dirhodium dfpma photocycle for H_2 production from a homogeneous HX solution employing a two-electron mixed-valence $Rh_2^{0,II}$ core. Thermal ellipsoids are drawn at the 50% probability level, and the $-CH_2CF_3$ groups and the bridgehead N−Me and hydrogens of the tfepma and tfepm ligands have been omitted for clarity.

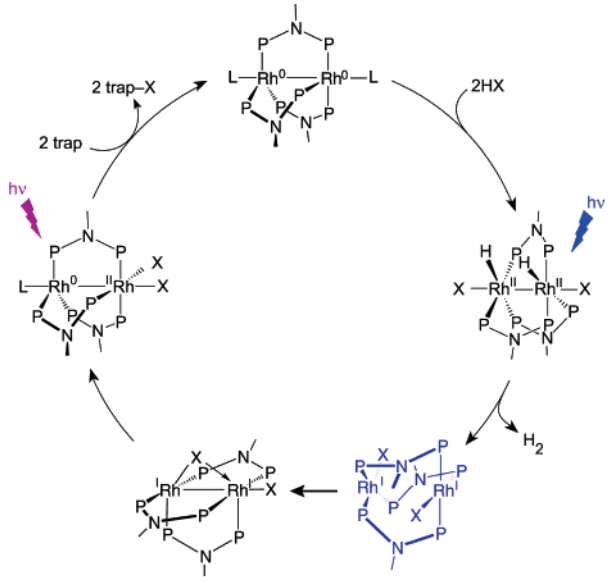

Figure 6. Complete photocycle for H_2 generation by the dirhodium dfpma photocatalyst. Identification of the intermediates in the cycle is based on the chemistry of dirhodium and diiridium tfepma and tfepm synthetic analogues.

gold for M−X activation. Initial results in this area are described below.

2.4. Bimetallic Gold Complexes for the Photoactivation of M−X Bonds. Gold complexes possess a number of promising properties for the purposes of M−X bond photoactivation. First, dimers of gold are available with the metal in the 1+, 2+, and 3+ oxidation states. The Au^{III} oxidation state is quite oxidizing with a textbook $Au^{III/I}$ reduction potential (1.36 V vs SHE in acidic solution)[53] that is commensurate with halogen oxidation. Although the reduction potential is highly dependent on its ligand environment, as well as the solvent used, it is clear that Au^{III} is a very oxidizing metal center. Second, the coordination geometries of an $Au^{III/I}$ couple are well suited for halogen elimination: Au^{I} adopts a linear geometry, whereas Au^{III} typically is square planar. This decrease in the coordination number by 2 with the attendant two-electron reduction of the gold center is well matched to the desired two-electron oxidative addition/reductive elimination chemistry required for halogen photoactivation. Third, two-electron mixed valency of digold centers already has been observed by Fackler[54] and

(53) Schmid, G. M. In *Standard Potentials in Aqueous Solutions*; Bard, A. J., Parsons, R., Jordan, J., Eds.; IUPAC, Marcel Dekker: New York, 1985; pp 313−320.
(54) Fackler, J. P., Jr. *Inorg. Chem.* **2002**, *41*, 6959−6972.

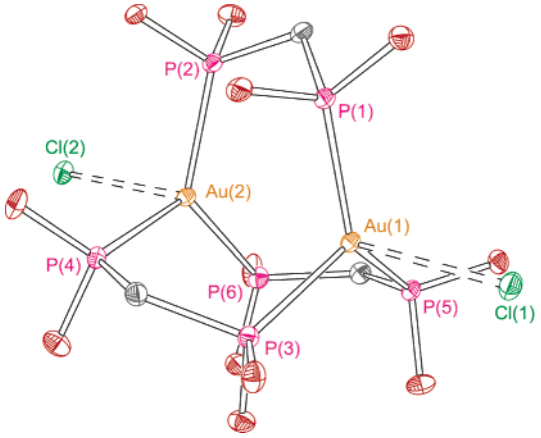

Figure 7. Solid-state structure of $Au_2(tfepm)_3Cl_2$ (**12**). Thermal ellipsoids are drawn at the 50% probability level, and $-CH_2CF_3$ groups and bridge hydrogens of the tfepm ligand have been omitted for clarity.

Grohmann and Schmidbaur,[55] who have prepared a $Au^I\cdots Au^I$, $Au^{II}-Au^{II}$, $Au^I\cdots Au^{III}$, and $Au^{III}\cdots Au^{III}$ series bridged by anionic phosphorus ylide ligands. Conversion between these complexes proceeds exclusively in two-electron steps. Finally, although $Au^I\cdots Au^{III}$ does not possess a formal metal−metal bond, the compound has an allowed, low-energy $d\sigma^* \rightarrow p\sigma$ transition.[56] Thus, as with the dirhodium mixed-valence complexes, an electronic transition related to a metal−metal bond is retained as a potential chromophore, from which M−X photoactivation may be initiated.

We have sought to elaborate a coordination chemistry of digold centers akin to that observed for the rhodium and iridium bimetallics. A digold core bridged by three tfepm ligands, $Au_2(tfepm)_3Cl_2$ (**12**), may be assembled according to the following reaction:

$$2AuCl(THT)\ (THT = \text{tetrahydrothiophene}) + 3\ tfepm \rightarrow Au_2(tfepm)_3Cl_2 \quad (4)$$

As shown in Figure 7, a three-coordinate planar geometry, similar to that observed for $Rh_2^{0,0}$ dfpma and tfepma complexes, is obtained as opposed to the linear geometry more typical of Au^I. The trigonal geometry for Au^I has been observed in only one other structurally characterized bis(phosphino)methane-bridged complex, namely, that of $Au_2(dmpm)_3(BF_4)_2$ [dmpm = bis(dimethylphosphino)-methane].[57] The Au···Au distance of 3.5295(7) Å in **12** is markedly longer than the 3.045 Å Au···Au distance observed in $Au_2(dmpm)_3(BF_4)_2$ and likely arises from the association of the chloride anions in the former. Digold complex **12** will allow for the examination of M−X photoactivation pending the outcome of its oxidation reactivity, which is currently under investigation.

We ultimately would like to couple the hydrogen production properties of dirhodium centers with the halogen elimination that we are developing for digold complexes. Toward this end, we have begun exploring mixed-metal gold−rhodium complexes. We have synthesized the mixed-metal complex $[Au^IRh^I(^tBuNC)_2(dppm)_2]Cl_2$ (**13**) (dppm = bis(diphenylphosphino)methane), which has been previously prepared with other anions[58] but not structurally characterized. The structure of the hetero-bimetallic compound shown in Figure 8 displays a nearly square-planar Rh^I center, with two trans-disposed *tert*-butyl isocyanide groups and bridging dppm ligands ($\angle P-Rh-P = 173.01°$) comprising the primary coordination sphere. The other ends of the dppm ligands coordinate the Au^I center in a linear geometry ($\angle P-Au-P = 174.99°$). The $Au^I\cdots Rh^I$ interatomic distance of 2.9214(9) Å is slightly longer than the 2.854 Å average distance reported for the only other structurally characterized $Au^I\cdots Rh^I$ species, $AuRh(PNP)_2(BF_3NO_3)$ (here PNP = 2-[bis(diphenylphosphino)methyl]pyridine]).[59] For the case of **13**, the chloride anions are not associated with the metal centers. Current efforts are focused on reducing this complex to a $Rh^0\cdots Au^I$ core, the formation of which should be driven by partial metal−metal bond formation. We believe that the resulting $Rh^0\cdots Au^I$ species will provide an entry point into HX photocatalysis because $(H)_2Rh^{II}-Au^{III}(X)_2$ species are available, in principle, by the oxidative addition of 2 equiv of HX. We are currently examining the feasibility of forming such a species, which will allow M−X photoactivation to occur from a highly oxidizing Au^{III} center and H_2 elimination to proceed, as observed previously, from a Rh^{II} center.

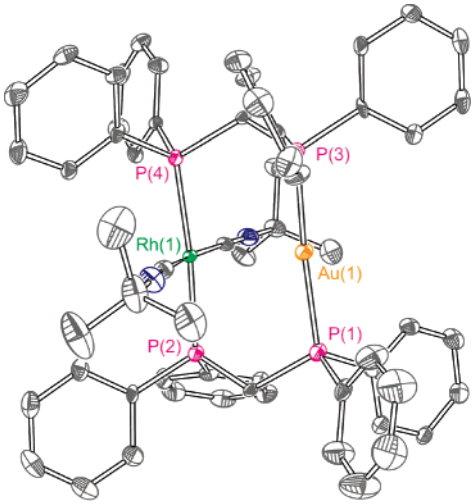

Figure 8. Solid-state structure of $Au^IRh^I(^tBuNC)_2(dppm)_2Cl_2$ (**13**). Thermal ellipsoids are drawn at the 40% probability level.

3. Oxygen Photoproduction

The oxidation half of the water-splitting problem presents an even greater challenge than the reduction side because the basic chemical principles that drive O−O bond coupling are extremely complex (vide infra). The need to understand a number of essential science issues is underscored with the recently reported structure of the oxygen-evolving complex

(55) Grohmann, A.; Schmidbauer, H. In *Comprehensive Organometallic Chemistry, II*; Abel, E. W., Stone, F. G. A., Wilkinson, G., Eds.; Pergamon: New York, 1995; Vol. 3, pp 1−56.
(56) Forward, J. M.; Fackler, J. P., Jr.; Assefa, Z. In *Optoelectronic Properties of Inorganic Compounds*; Roundhill, D. M., Fackler, J. P., Jr., Eds.; Plenum Press: New York, 1999; Chapter 6, pp 195−229.
(57) Bensch, W.; Prelati, M.; Ludwig, W. *J. Chem. Soc., Chem. Commun.* **1986**, 1762−1763.
(58) Langrick, C. R.; Shaw, B. L. *Dalton Trans.* **1985**, 511−516.
(59) McNair, R. J.; Nilsson, P. V.; Pignolet, L. H. *Inorg. Chem.* **1985**, *24*, 1935−1939.

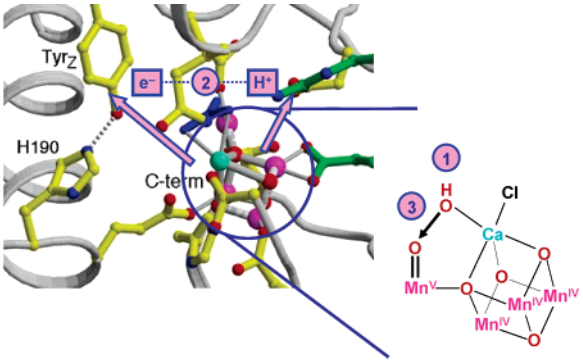

Figure 9. Structure (3.4 Å resolution) of the OEC adapted from ref 62 and a proposed oxidation state model for O−O bond coupling. The numbering indicates challenges overcome by PSII in performing the water-splitting reaction: (1) the use of the protein structure to control the active-site primary and secondary coordination spheres to bring two water molecules together; (2) the divergent PCET pathway, indicating the exit channels for electrons and protons; and (3) the O−O bond-forming reaction, which involves an extensive reaction chemistry beyond simple electron transfer (see text).

(OEC) and accompanying protein environment of photosystem II (PSII). As researchers continue their drive toward obtaining higher resolution structures,[60,61] a working model for the mechanism of water splitting at the OEC is beginning to emerge.

Figure 9 shows the results of the highest resolution structure of PSII to date.[62] A cubane-like Mn_3CaO_4 cluster is proposed in which metals are held together by μ-oxo bridges.[62,63] The X-ray structure is consistent with the "3 + 1" configuration of Mn centers deduced from EXAFS[64] and ENDOR[65,66] experiments. The key intermediate in the critical bond-forming step of water oxidation is a preorganized oxo/hydroxyl intermediate. The O−O bond-making reaction effectively involves a nucleophilic attack of hydroxide on an electrophilic oxygen, a transformation now incorporated in most current mechanisms for O_2 generation at the OEC.[67−70] The Ca^{2+} ion is thought to decrease the pK_a of an unbound water to produce a noncoordinated and nucleophilic hydroxide that attacks the electrophilic oxo of a high-valent manganese.[67,69,70] The chemical challenges confronting the development of a functional model for water splitting are labeled in Figure 9:

1. Architectures must be defined that permit control of the secondary coordination environment to preassemble two water molecules prior to coupling.

2. Water must be activated by coupling proton-transfer reactions to multielectron redox chemistry. Hence, new experiments must be designed that permit such PCET reactions to be defined. At the cluster active site, the two waters are activated to generate the critical oxo/hydroxo intermediate by a series of PCET events. The removal of electrons and protons from the OEC is assuredly related to the Kok cycle for water activation by PSII.[68,71−74] The electron and proton inventory is managed away from the active site by the protein environment. Models prior to the crystal structure proposed congruent PCET channels in which the activation of the infamous Tyr_Z (Y161)[75−79] occurred by proton transfer away from the OEC active site were mediated by H190.[80] However, the crystal structure[62] has refined this picture as Figure 9 indicates. The proton output channel, identified in the crystal structure to begin at D61, is orthogonal to the electron output channel, which proceeds through Tyr_Z. The crystal structure shows that tyrosine oxidation most likely proceeds by a proton transfer between Tyr_Z and H190, which is isolated and not part of a proton-transfer exit channel.

3. Development of rational and predictable methodologies for the formation of O−O bonds, which involves basic reaction types that are not yet controllable or predictable, at least not to the extent that Marcus theory has provided to our understanding of one-electron redox reactions. The O−O bond-forming step involves a *multielectron* process and *atom transfer* of oxygen from a strong metal−oxo bond. Moreover, the multielectron process is likely *proton-coupled*. The O−O bond-forming step thus embodies a reactivity suite that steps well beyond single-electron transfer.

Described below are our systematic efforts to address challenges 1−3 in the contextual framework of the water-splitting reaction.

3.1. Water Assembly by Controlling Secondary Coordination Spheres. Our first generation approach to the water assembly, challenge 1, focused on bisporphyrins arranged in a cofacial orientation by a single rigid pillar. The approach builds on the designs of Collman and Chang, who utilized

(60) Barber, J. *Biochim. Biophys. Acta* **2004**, *1655*, 123−132.
(61) Barber, J.; Ferreira, K.; Maghlaoui, K.; Iwata, S. *Phys. Chem. Chem. Phys.* **2004**, *6*, 4737−4742.
(62) Ferreira, K. N.; Iverson, T. M.; Maghlaoui, K.; Barber, J.; Iwata, S. *Science* **2004**, *303*, 1831−1838.
(63) Iwata, S.; Barber, J. *Curr. Opin. Struct. Biol.* **2004**, *14*, 447−453.
(64) Robblee, J. H.; Messinger, J.; Cinco, R. M.; McFarlane, K. L.; Carmen Fernandez, C.; Pizarro, S. A.; Sauer, K.; Yachandra, V. K. *J. Am. Chem. Soc.* **2002**, *124*, 7459−7471.
(65) Peloquin, J. M.; Campbell, K. A.; Randall, D. W.; Evanchik, M. A.; Pecoraro, V. L.; Armstrong, W. H.; Britt, R. D. *J. Am. Chem. Soc.* **2000**, *122*, 10926−10942.
(66) Britt, R. D.; Campbell, K. A.; Peloquin, J. M.; Gilchrist, M. L.; Aznar, C. P.; Dicus, M. M.; Robblee, J.; Messinger, J. *Biochim. Biophys. Acta* **2004**, *1655*, 158−171.
(67) Vrettos, J. S.; Limburg, J.; Brudvig, G. W. *Biochim. Biophys. Acta* **2001**, *1503*, 229−245.
(68) Tommos, C.; Babcock, G. T. *Acc. Chem. Res.* **1998**, *31*, 18−25.
(69) Pecoraro, V. L.; Baldwin, M. J.; Caudle, M. T.; Hsieh, W. Y.; Law, N. A. *Pure Appl. Chem.* **1998**, *70*, 925−929.
(70) Messinger, J.; Badger, M.; Wydrzynski, T. *Proc. Natl. Acad. Sci. U.S.A.* **1995**, *92*, 3209−3213.
(71) Hoganson, C. W.; Babcock, G. T. *Science* **1997**, *277*, 1953−1956.
(72) Babcock, G. T.; Barry, B. A.; Debus, R. J.; Hoganson, C. W.; Atamian, M.; McIntosh, L.; Sithole, I.; Yocum, C. F. *Biochemistry* **1989**, *28*, 9557−9565.
(73) Westphal, K. L.; Tommos, C.; Cukier, R. I.; Babcock, G. T. *Curr. Opin. Plant Biol.* **2000**, *3*, 236−242.
(74) Tommos, C. *Philos. Trans. R. Soc. London, Ser. B* **2002**, *357*, 1383−1394.
(75) Barry, B. A.; Babcock, G. T. *Proc. Natl. Acad. Sci. U.S.A.* **1987**, *84*, 7099−7103.
(76) Debus, R. J.; Barry, B. A.; Babcock, G. T.; McIntosh, L. *Proc. Natl. Acad. Sci. U.S.A.* **1988**, *85*, 427−430.
(77) Debus, R. J.; Barry, B. A.; Sithole, I.; Babcock, G. T.; McIntosh, L. *Biochemistry* **1988**, *27*, 9071−9074.
(78) Diner, B.; Schlodder, E.; Nixon, P. J.; Coleman, W. J.; Rappaport, F.; Vermaas, W. F. J.; Chisholm, D. A. *Biochemistry* **2001**, *40*, 9265−9281.
(79) Vermaas, W. F. J.; Rutherford, A. W.; Hansson, O. N. *Proc. Natl. Acad. Sci. U.S.A.* **1988**, *85*, 8477−8481.
(80) Hoganson, C. W.; Pressler, M. A.; Proshlyakov, D. A.; Babcock, G. T. *Biochim. Biophys. Acta* **1998**, *1365*, 170−174.

anthracene (DPA) and biphenylene (DPB) pillars to juxtapose cofacial bisporphyrins.[81−84] These systems, designated "Pacman" porphyrins, have been prominent electrocatalysts for the reduction of oxygen to water (the microscopic reverse of O_2 formation) when the porphyrin contains late transition metals (e.g., Co).[84] However, the cofacial motif poses a problem for porphyrins containing earlier transition metals such as Fe and Mn, which are best-suited for oxygen atom coupling. The high thermodynamic driving force for M_2 μ-oxo formation is a significant impediment to the water

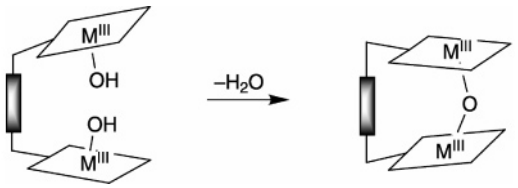

(5)

assembly problem. We therefore engineered new cofacial bisporphyrins displaying expanded pockets with the goal of hindering μ-oxo formation. In the DPX (diporphyrin xanthene) and DPD (diporphyrin dibenzofuran) cofacial constructs of Figure 10,[85,86] neighboring porphyrins display an extensive range of vertical pocket size dimensions and flexibilities with minimal lateral displacement between macrocycle subunits. By employment of the appropriate substituents along the periphery of the macrocycle superstructure, it is possible to tune the pocket sizes of the Pacman motif in increments of 0.5 Å over a series of metal−metal distances ranging from 3.5 to over 8.5 Å.[87−89] Similar to DPA and DPB Pacman porphyrins, the dicobalt(II) complexes of both DPX and DPD are effective electrocatalysts for the direct four-electron, four-proton reduction of oxygen to water over the more common two-electron, two-proton reduction to hydrogen peroxide.[90,91] However, comparative structural,[92] steady-state reactivity,[93,94] and time-resolved spectroscopy[95]

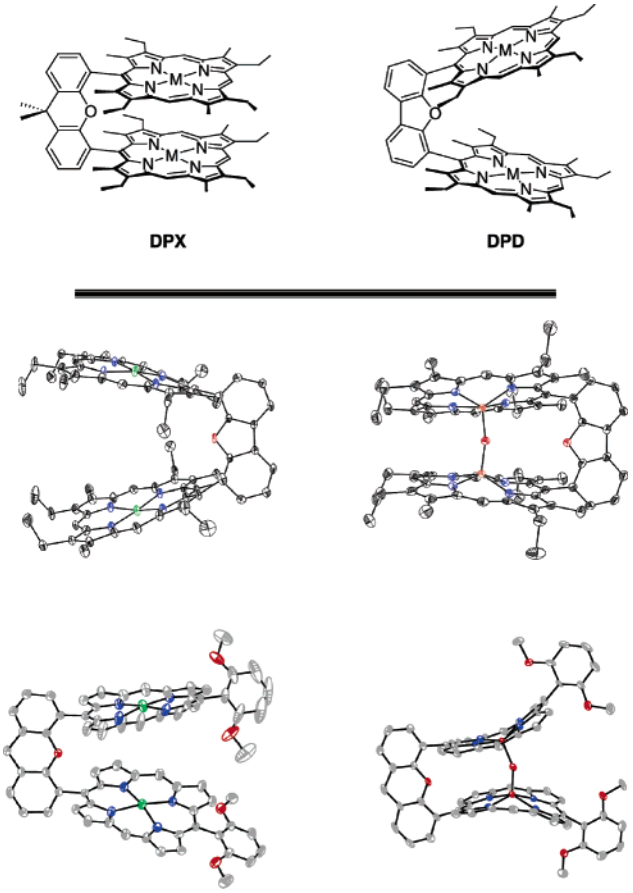

Figure 10. (Top) Molecular structures of the DPX and DPD cofacial bisporphyrins. Crystal structures of open Zn (left) and closed Fe_2 μ-oxo (right) forms of the DPD (middle) and DPXM (bottom) Pacman bisporphyrins.

studies reveal that neither large vertical pocket sizes nor substituents around the porphyrin periphery impede μ-oxo formation. As shown in Figure 10, the Fe_2 μ-oxo core may form either by the unprecedented flexibility of the DPD system to open and close its binding pocket by a vertical distance of over 4 Å or by distortion of the macrocycle ring of the sterically encumbered DPXM system (methoxyaryl groups at meso positions trans to the xanthene spacer).

In the absence of a metal to coordinate water, the challenge for this step is to control the secondary coordination sphere so that a water (and accordingly incipient hydroxide) is present for nucleophilic attack. We have addressed the challenging task of secondary sphere organization of water above a redox platform by designing Hangman porphyrins in which a "hanging" acid−base group poises a water molecule above a redox platform.[96] In the absence of the second metal, μ-oxo formation is prevented.

The crystal structure of the xanthene Hangman (HPX) iron porphyrin is shown in Figure 11.[97] The complex represents the first structurally characterized monomeric iron(III) hydroxide porphyrin. As intended in its original design, a water molecule is suspended between the xanthene carboxylic

(81) Chang, C. K.; Abdalmuhdi, I. *J. Org. Chem.* **1983**, *48*, 5388−5390.
(82) Chang, C. K.; Abdalmuhdi, I. *Angew. Chem., Int. Ed. Engl.* **1984**, *23*, 164−165.
(83) Collman, J. P.; Hutchison, J. E.; Lopez, M. A.; Tabard, A.; Guilard, R.; Seok, W. K.; Ibers, J. A.; L'Her, M. *J. Am. Chem. Soc.* **1992**, *114*, 9869−9877.
(84) Collman, J. P.; Wagenknecht, P. S.; Hutchison, J. E. *Angew. Chem., Int. Ed. Engl.* **1994**, *33*, 1537−1554.
(85) Chang, C. J.; Deng, Y.; Heyduk, A. F.; Chang, C. K.; Nocera, D. G. *Inorg. Chem.* **2000**, *39*, 959−966.
(86) Chang, C. J.; Baker, E. A.; Pistorio, B. J.; Deng, Y.; Loh, Z.-H.; Miller, S. E.; Carpenter, S. D.; Nocera, D. G. *Inorg. Chem.* **2002**, *41*, 3102−3109.
(87) Chang, C. J.; Deng, Y.; Peng, S. M.; Lee, G. H.; Yeh, C. Y.; Nocera, D. G. *Inorg. Chem.* **2002**, *41*, 3008−3016.
(88) Chng, L. L.; Chang, C. J.; Nocera, D. G. *J. Org. Chem.* **2003**, *68*, 4075−4078.
(89) Chang, C. J.; Loh, Z.-H.; Deng, Y.; Nocera, D. G. *Inorg. Chem.* **2003**, *42*, 8262−8269.
(90) Chang, C. J.; Deng, Y.; Shi, C.; Chang, C. K.; Anson, F. C.; Nocera, D. G. *Chem. Commun.* **2000**, 1355−1356.
(91) Chang, C. J.; Loh, Z.-H.; Shi, C.; Anson, F. C.; Nocera, D. G. *J. Am. Chem. Soc.* **2004**, *126*, 10013−10020.
(92) Deng, Y.; Chang, C. J.; Nocera, D. G. *J. Am. Chem. Soc.* **2000**, *122*, 410−411.
(93) Pistorio, B. J.; Chang, C. J.; Nocera, D. G. *J. Am. Chem. Soc.* **2002**, *124*, 7884−7885.
(94) Rosenthal, J.; Pistorio, B. J.; Chng, L. L.; Nocera, D. G. *J. Org. Chem.* **2005**, *70*, 1885−1888.
(95) Hodgkiss, J. M.; Chang, C. J.; Pistorio, B. J.; Nocera, D. G. *Inorg. Chem.* **2003**, *42*, 8270−8277.
(96) Chang, C. J.; Yeh, C. Y.; Nocera, D. G. *J. Org. Chem.* **2002**, *67*, 1403−1406.
(97) Yeh, C. Y.; Chang, C. J.; Nocera, D. G. *J. Am. Chem. Soc.* **2001**, *123*, 1513−1514.

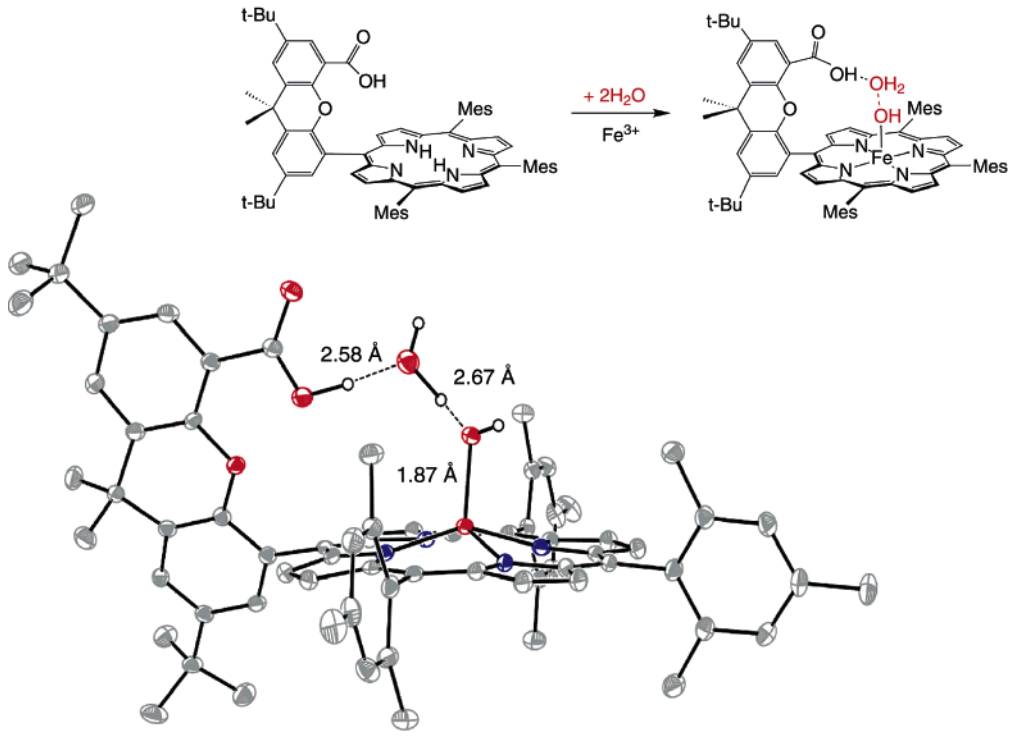

Figure 11. (Top) Schematic for the introduction of two waters into the cleft of the Hangman architecture. (Bottom) Crystal structure of Hangman porphyrin showing a molecule of water suspended over a metal-bound hydroxide (formally from the addition of a second molecule of water).

acid hanging group and the hydroxide ligand. This is the first synthetic redox-active site displaying an assembled water molecule as part of a structurally well-defined proton-transfer network. Spectroscopic data for (HPX)Fe^{III}OH indicate that the water molecule remains bound in solution as well as in the solid state and that this binding is chemically reversible. The measured binding energy of the water molecule within the Hangman cleft is 5.8 kcal/mol.[98] The HPX platform thus provides a microcavity for examination of O−O bond formation by juxtaposing two oxygen atoms between proton- and electron-transfer sites.

3.2. PCET: Mechanism and Oxygen Activation. A crucial element to the success of water splitting at OEC entails the coupling of electron and proton transport to activate OEC and, in turn, water. An understanding of PCET was launched at a mechanistic level by our studies of D- - -[H$^+$]- - -A (D = donor, A = acceptor, and [H$^+$] = proton-transfer interface) systems.[99] Initial systems were designed to emphasize the collinear geometry shown in Figure 12a.[100] A hydrogen-bond interface is used to preorganize electron donor/acceptor (D/A) pairs. Electron transfer between D/A pairs is necessarily modulated by the presence of a proton. These systems have provided tangible kinetics benchmarks for PCET reactions[101−107] and stimulated the

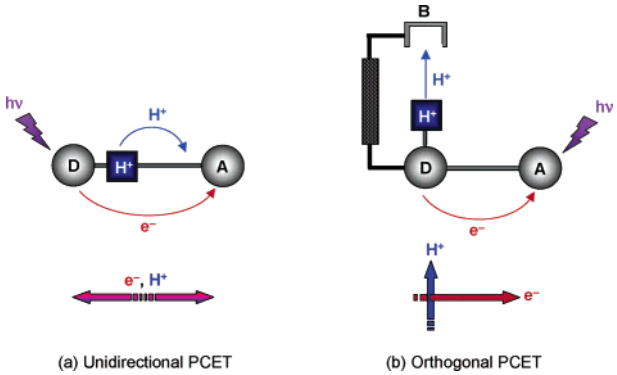

Figure 12. PCET assemblies used for mechanistic investigations of PCET where the electron and proton transport occur along (a) collinear and (b) orthogonal pathways.

developmentof theories to describe PCET.[12,108,109] The key ingredients that determine the rate of any charge-transfer reaction, the activation energy, and the electronic coupling, depend on both the proton and electron coordinates in a

(98) Chang, C. J.; Chng, L. L.; Nocera, D. G. *J. Am. Chem. Soc.* **2003**, *125*, 1866−1876.
(99) Turró, C.; Chang, C. K.; Leroi, G. E.; Cukier, R. I.; Nocera, D. G. *J. Am. Chem. Soc.* **1992**, *114*, 4013−4015.
(100) Chang, C. J.; Brown, J. D. K.; Chang, M. C. Y.; Baker, E. A.; Nocera, D. G. In *Electron Transfer in Chemistry*; Balzani, V., Ed.; Wiley-VCH: Weinheim, Germany, 2001; Vol. 3.2.4, pp 409−461.
(101) Yeh, C. Y.; Miller, S. E.; Carpenter, S. D.; Nocera, D. G. *Inorg. Chem.* **2001**, *40*, 3643−3646.
(102) Damrauer, N. H.; Hodgkiss, J. M.; Rosenthal, J.; Nocera, D. G. *J. Phys. Chem. B* **2004**, *108*, 6315−6321.
(103) Roberts, J. A.; Kirby, J. P.; Nocera, D. G. *J. Am. Chem. Soc.* **1995**, *117*, 8051−8052.
(104) Deng, Y.; Roberts, J. A.; Peng, S. M.; Chang, C. K.; Nocera, D. G. *Angew. Chem., Int. Ed. Engl.* **1997**, *36*, 2124−2127.
(105) Roberts, J. A.; Kirby, J. P.; Wall, S. T.; Nocera, D. G. *Inorg. Chim. Acta* **1997**, *263*, 395−405.
(106) Kirby, J. P.; van Dantzig, N. A.; Chang, C. K.; Nocera, D. G. *Tetrahedron Lett.* **1995**, *36*, 3477−3480.
(107) Kirby, J. P.; Roberts, J. A.; Nocera, D. G. *J. Am. Chem. Soc.* **1997**, *119*, 9230−9236.
(108) Hammes-Schiffer, S. In *Electron Transfer in Chemistry*; Balzani, V., Ed.; Wiley-VCH: Weinheim, Germany, 2001; Vol. 1.1.5, pp 189−237.
(109) Hammes-Schiffer, S. *Acc. Chem. Res.* **2001**, *34*, 273−281.

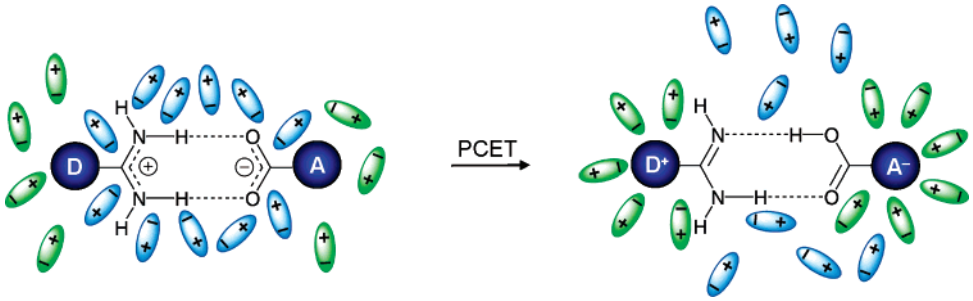

Figure 13. Schematic representation of the dipole rearrangement of the external environment after a PCET event.

PCET reaction. This coupling of the charge shift resulting from electron and proton motion to the polarization of the surrounding environment, schematically represented in Figure 13, is a distinguishing characteristic of a PCET reaction. This mechanism lies at the heart of biological energy conversion,[110] especially those deriving their function from radical transport.[111−115]

The relation of PCET to substrate activation, including oxygen, is under investigation by developing the construct shown in Figure 12b. The overall architecture is embodied by the Hangman platform, which is a nexus for electron- and proton-transfer events. The approach is powerful because it separates electron- and proton-transfer coordinates, thus allowing for the independent study of energetics and distance dependences of the electron- and proton-transfer events. For instance, by simply interposing a water molecule near the HPX spacer, we can switch from a configuration requiring one long-distance proton-transfer event (∼3.5 Å) coupled to electron transfer to one requiring two short-distance proton-transfer events (1.8 Å, proton hopping along a water chain). This orthogonalization of electron- and proton-transfer pathways captures a key feature of PCET in nature. Because the proton is a heavy particle, its tunneling rate drops off quickly with distance as compared to an electron.[116] Accordingly, the redox cofactors of many enzymes are hard-wired to a proton network that is derived from a structured water channel or from secondary amino acid side chains. Protons can hop over short distances, and thus rates of proton transfer can be commensurate with longer-distance electron-transfer events. In this way, coupling between the electron and proton can be achieved.

Inasmuch as the activation of oxygen and water in biology inexorably involves PCET events, proton-transfer networks orthogonalized to redox cofactors are an especially prevalent structural motif for enzymes that derive their function from oxygen activation. The structures of cytochrome P450 and

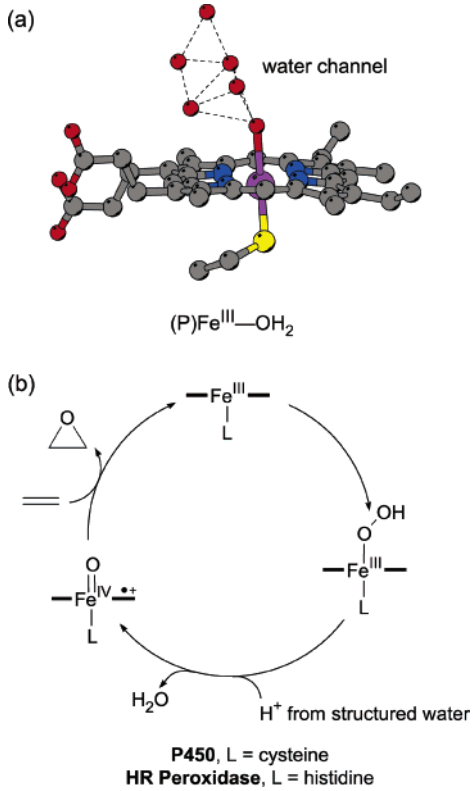

Figure 14. (a) High-resolution structure of cytochrome P450, displaying a water channel above the heme. (b) Peroxo shunt mechanism of mono-oxygenases producing compound I ($(P^{\bullet+})Fe^{IV}$═O), which oxidizes substrates by their nucleophilic attack on the electrophilic oxo of the $(P^{\bullet+})Fe^{IV}$═O core.

mono-oxygenases are exemplary in this respect. Figure 14a shows the structure of the former.[117] Protons are managed by the water channel, which is directed along the coordination axis of oxygen activation. The highly activated ferryl oxygen of the redox cofactor, $P^{\bullet+}Fe^{IV}$═O (compound I-type intermediate in which an Fe^{IV}═O center resides in a porphyrin cation radical, $P^{\bullet+}$), is produced by proton transfer from the water channel to a ferric peroxy intermediate, as shown in Figure 14b. Formation of the high-valent metal oxo fragment is thus accomplished by coupling proton transfer to an internal $2e^-$ redox event.

We have found that the protonic pendant acid group of the Hangman porphyrin plays the same role as the water channels of natural enzymes. Proton transfer from the acid−base hanging group in $(HPX)Fe^{III}$ peroxide complexes yields

(110) Stubbe, J.; Nocera, D. G.; Yee, C. S.; Chang, M. C. Y. *Chem. Rev.* **2003**, *103*, 2167−2201.
(111) Chang, M. C. Y.; Yee, C. S.; Stubbe, J.; Nocera, D. G. *Proc. Natl. Acad. Sci. U.S.A.* **2004**, *101*, 6882−6887.
(112) Yee, C. S.; Chang, M. C. Y.; Ge, J.; Nocera, D. G.; Stubbe, J. *J. Am. Chem. Soc.* **2003**, *125*, 10506−10507.
(113) Reece, S. Y.; Stubbe, J.; Nocera, D. G. *Biophys. Biochim. Acta* **2005**, *1706*, 232−238.
(114) Chang, M. C. Y.; Yee, C. S.; Nocera, D. G.; Stubbe, J. *J. Am. Chem. Soc.* **2004**, *126*, 16702−16703.
(115) Yee, C. S.; Seyedsayamdost, M. R.; Chang, M. C. Y.; Nocera, D. G.; Stubbe, J. *Biochemistry* **2003**, *42*, 14541−14542.
(116) Krishtalik, L. I. *Charge-transfer reactions in electrochemical and chemical processes*; Plenum: New York, 1979.
(117) Poulos, T. L.; Finzel, B. C.; Howard, A. J. *Biochemistry* **1986**, *25*, 5314−5322.

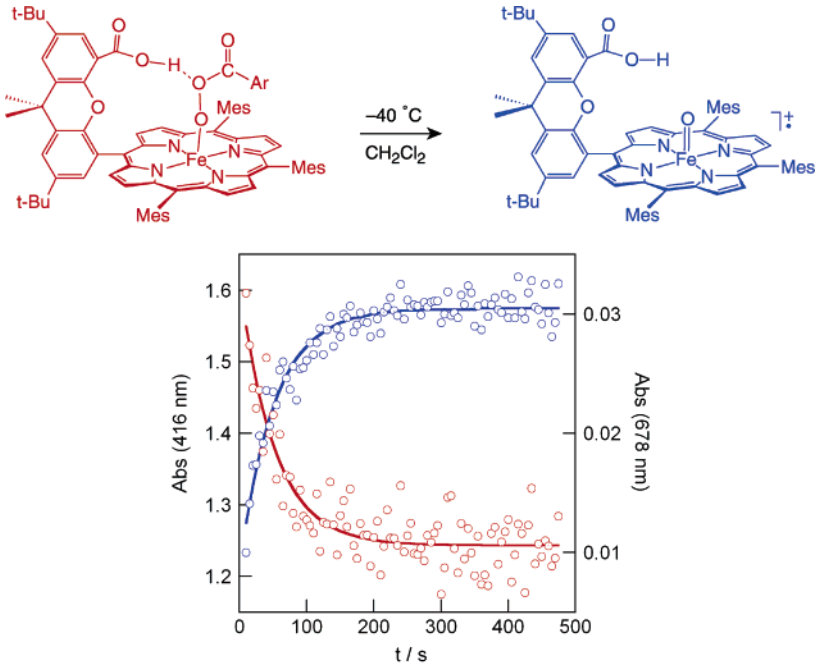

Figure 15. Selected stopped-flow data for the disappearance (red) of (HPX)Fe^{III} acyl peroxide (λ_{max} = 416 nm[118]) and the concomitant appearance (blue) of ($HP^{\bullet+}X$)Fe^{IV}=O (λ_{max} = 678 nm[118]). Global analysis of the full spectral window (400−700 nm) for the disappearance and appearance traces using a first-order kinetic model gives $k_{obs} = (1.9 \pm 0.1) \times 10^{-2}$ s^{-1} for O−O bond heterolysis.

Scheme 3

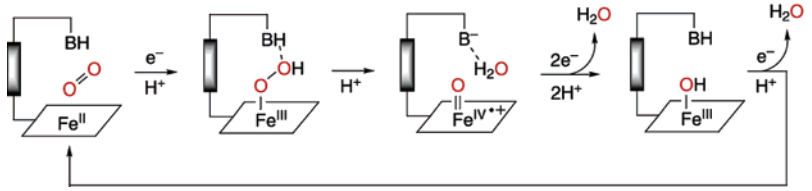

($HP^{\bullet+}X$)Fe^{IV}=O. Figure 15 shows the stopped-flow kinetics for a reaction of (HPX)Fe^{III}(OH) and *m*-chloroperoxybenzoic acid (*m*-CPBA) in CH_2Cl_2 at −40 °C. Substitution of a perbenzoate for hydroxide first affords a ferric acylperoxo species in seconds. The absorption spectrum of the acyl peroxide (λ_{max} = 416 and 506 nm[118]) smoothly disappears with the concomitant growth of the absorption spectrum for ($HP^{\bullet+}X$)Fe^{IV}=O (λ_{max} = 678 nm[118]). No intermediates are observed in the process, thereby indicating exclusive O−O bond heterolysis, a $2e^-$ redox event coupled to intramolecular proton transfer, as is the case for cytochrome P450 and other mono-oxygenases. A properly positioned acid−base residue, in fact, works to facilitate such internal multielectron chemistry while inhibiting single-electron processes. Homolytic O−O bond cleavage—a $1e^-$, $1H^+$ transformation—is suppressed by the pillared acid unit in reactions that otherwise afford O−O homolysis on porphryin scaffolds that cannot support proton transfer. This result is of pertinence to the water-splitting reaction because it shows that a highly electrophilic oxo can be supported on a Hangman platform. It additionally provides direct mechanistic insights into the effects of a controlled secondary coordination sphere in *multielectron PCET* reactions toward challenges 2 and 3. The presentation of the oxo in a Hangman cleft possesses some of the salient features of the OEC in PSII.

3.3. O−O Bond Formation. The electrophilic oxo of the Hangman platform exhibits reactivity patterns essential for water activation. The oxo reacts with peroxide in a dismutation reaction to produce oxygen and water.[119] Under electrocatalytic reducing conditions, the Hangman porphyrin reacts with oxygen to produce water by the mechanism proposed in Scheme 3, which is consistent with the stopped-flow results of Figure 15. Scheme 3 is important to the goals of water splitting because the conversion is the microscopic reverse of the O−O bond-forming chemistry that is needed for water oxidation. We have initially addressed the reverse bond-formation step by examining the nucleophilic attack of olefins on the electrophilic oxo of $P^{\bullet+}Fe^{IV}$=O (Scheme 4). The production of an epoxide entails a two-electron transfer of an oxygen atom from the porphyrin platform to an olefin.[120,121] In the presence of an external peroxide source, the reaction is catalytic and proceeds with high turnover numbers.

(118) Groves, J. T.; Watanabe, Y. *J. Am. Chem. Soc.* **1988**, *110*, 8443−8452.
(119) Chng, L. L.; Chang, C. J.; Nocera, D. G. *Org. Lett.* **2003**, *5*, 2421−2424.
(120) Kaizer, J.; Klinker, E. J.; Oh, N. Y.; Rohde, J.-U.; Song, W. J.; Stubna, A.; Kim, J.; Munck, E.; Nam, W.; Que, L., Jr. *J. Am. Chem. Soc.* **2004**, *126*, 472−473.
(121) Groves, J. T.; Gross, A.; Stern, M. K. *Inorg. Chem.* **1994**, *33*, 5065−5072.

Scheme 4

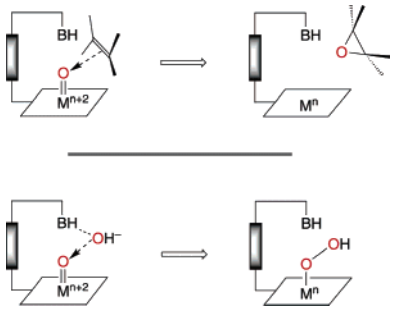

To effect water splitting, as indicated in Scheme 4, the olefinic nucleophile needs to be replaced by hydroxide. Practically, OH^- is thermodynamically more difficult to oxidize than olefins, and hence the electrophilicity of the oxo of $(HP^{\bullet+}X)Fe^{IV}{=}O$ needs to be maximized. Moreover, the proton inventory of the current HPX platform is incompatible for the formation and stabilization of nucleophilic hydroxide from a suspended water molecule. The carboxylic acid hanging group of the Hangman architecture needs to be replaced with a Brønsted−Lowry base to generate the required hydroxide nucleophile.

Figure 16 shows a reconstructed Hangman platform for the water-splitting reaction. To boost the oxidation potential of the porphyrin subunit, we have added electron-withdrawing groups to the periphery of the porphyrin macrocycle. Introduction of ancillary fluorinated phenyl groups onto the meso positions of the porphyrin framework increases the oxidizing power of the porphyrin macrocycle by more than 0.4 V.[122,123] We are currently also exploring the fluorination of the β positions of the porphyrin ring to further augment the electron-withdrawing properties of the redox platform. β-Fluorine substitution of the porphyrin macrocycle has been shown to increase the oxidizing power of the redox subunit by roughly 0.5−0.6 V.[124] We have also developed a successful methodology for the incorporation of a wide variety of functional acid−base groups including amidine.[88] This hanging group has the same bond number connectivity as carboxylate, so it is geometrically matched to bind a water molecule in the Hangman cleft and is basic enough to generate the hydroxide nucleophile. Other electron-deficient platforms for the Hangman scaffold are also under examination. We have elaborated the Hangman strategy to salen and salophen ligands.[125] These platforms uniquely enrich our ability to explore the multielectron chemistry associated with water activation because their construction is highly modular, allowing two crucial components of the Hangman strategy as it pertains to water splitting—acid−base properties of the hanging group and redox properties of the platform—to be tuned with great synthetic facility.

We are currently evaluating the capacity of the Hangman platform shown in Figure 16 to promote O−O bond coupling by electrochemical techniques.[90,91] We have also turned our attention to introducing photooxidants onto the macrocycle. This approach provides us with a handle to photogenerate the critical high-valent oxo electrophile by flash quench photochemical methods[126] and, in doing so, opens the way to photochemically drive O−O bond formation. Toward this end, we have developed rhenium(I) polypyridyl complexes that contain an ancillary phosphine ligand through which electron transfer is directed.[127] Metal-to-ligand charge-transfer excitation promotes an electron from the Re^I center onto the polypyridine ligand. With the metal-to-ligand charge-transfer excited-state electron directed away from the phosphine, the highly oxidizing Re^{II} center can oxidize redox centers connected to the phosphine via a unidirectional electron cascade. In this way, an efficient and direct photooxidation of pendant redox centers may be achieved.[127] We are currently exploiting this strategy by attaching the phosphine of the rhenium(I) polypyridyl center to the meso position of the Hangman platform.

4. Concluding Remarks

Hydrogen and oxygen production from energy-poor substrates such as water involves *multielectron* processes that are *proton-coupled* for the *activation of kinetically inert and thermodynamically stable bonds.* We have made modest inroads to the foregoing italicized research areas by developing new types of excited-state molecules that connect to ground-state partners in multielectron steps and by developing a comprehensive approach to the investigation of PCET. With frameworks of multielectron chemistry and PCET in place, we have described a photocycle for hydrogen production from acidic solutions and developed new redox platforms that combine both electron and proton transfer for oxygen activation by atom transfer. We continue to expand on these basic reaction types with the aim of devising general principles that can be used in the design of transition-metal complexes for the activation of small molecules of energy consequence.

5. Experimental Section

5.1. General Procedures. All manipulations were carried out using modified Schlenk techniques under an atmosphere of N_2 or in a Vacuum Atmospheres HE-553-2 glovebox. Solvents for synthesis were of reagent grade or better and were purified and dried using a Braun solvent purification system or according to standard methods.[128] Bis[bis(trifluoroethoxy)phosphino]methane[129,130] and chloro(tetrahydrothiophene)gold(I)[131] were prepared according to literature methods. All other materials were used as received. Elemental analyses were performed at H. Kolbe Mikroanalytisches Laboratorium.

(122) Neya, S.; Funasaki, N. *J. Heterocycl. Chem.* **1997**, *34*, 689−690.
(123) Woller, E. K.; DiMagno, S. G. *J. Org. Chem.* **1997**, *62*, 1588−1593.
(124) Kadish, K. M.; Caemelbeck, E. V.; Royal, G. In *The Porphyrin Handbook*; Kadish, K. M., Smith, K. M., Guilard, R., Eds.; Academic Press: San Diego, CA, 2000; Vol. 8.
(125) Liu, S.-Y.; Nocera, D. G. *J. Am. Chem. Soc.* **2005**, *127*, 5278−5279.
(126) Connick, W. B.; Di Bilio, A. J.; Hill, M. G.; Winkler, J. R.; Gray, H. B. *Inorg. Chim. Acta* **1995**, *240*, 169−173.
(127) Reece, S. Y.; Nocera, D. G. *J. Am. Chem. Soc.* **2005**, *127*, 9448−9458.
(128) Armarego, W. L. F.; Perrin, D. D. *Purification of Laboratory Chemicals*, 4th ed.; Butterworth-Heinmann: Oxford, 1996.
(129) Hietkamp, S.; Sommer, H.; Stelzer, O. *Inorg. Synth.* **1989**, *27*, 120−121.
(130) Bitterwolf, T. E.; Raaghuveer, K. S. *Inorg. Chim. Acta* **1990**, *172*, 59−64.
(131) Uson, R.; Laguna, A.; Laguna, M. *Inorg. Synth.* **1989**, *26*, 85−91.

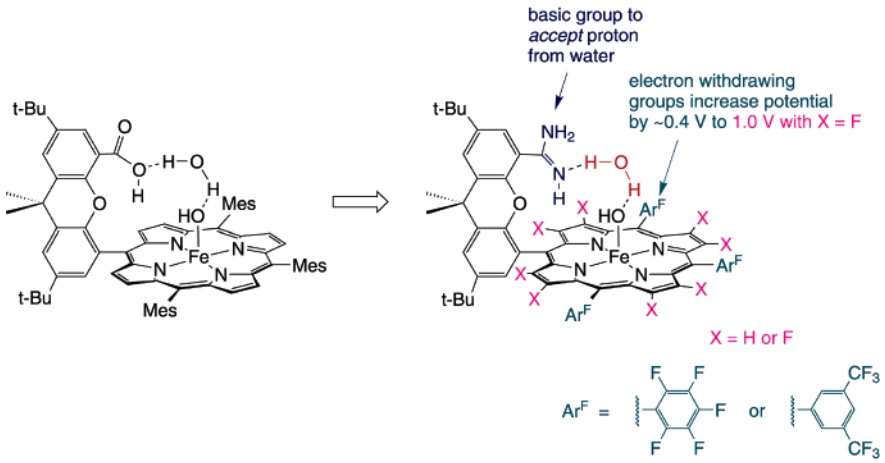

Figure 16. Redesign of the Hangman porphyrin platform from that of an O−O bond-breaking catalyst, Scheme 3, to one more suited for the investigation of O−O bond formation.

5.2. Synthesis of Dichlorotris{μ-{bis[bis(trifluoroethoxy)-phosphino]methane}}digold(I), $Au_2(tfepm)_3Cl_2$ (12). Chloro(tetrahydrothiophene)gold(I) (0.284 g, 0.883 mmol) was treated with 1.5 equiv of bis[bis(trifluoroethoxy)phosphino]methane (0.625 g, 1.324 mmol) in dichloromethane (8 mL) in a 20-mL scintillation vial, wrapped in foil to shield the contained solution from light. Though a white precipitate formed within 20 min, the reaction solution was left to stir for 2 h. The white precipitate was collected by filtration, yielding 0.549 g of **12** (66%). ^{1}H NMR (300 MHz, CD_3CN, 25 °C): δ 3.264 (s, 6 H), 4.835 (m, 24 H). ^{31}P{H} NMR (121.4 MHz, CD_3CN, 25 °C): δ 174.5.

5.3. Rhodium(I) Gold(I) Bis(*tert*-butylisonitrile)bis[μ-bis-(diphenylphosphino)methane] Dichloride (13). In a reaction vessel wrapped in foil to shield light, cyclooctadienerhodium(I) chloride dimer (0.100 g, 0.203 mmol) was treated with bis-(diphenylphosphino)methane (0.340 g, 0.885 mmol) in methylene chloride (5 mL), producing a red solution. A 2-mL methylene chloride solution of *tert*-butyl isocyanide (0.075 g, 0.903 mmol) was then added dropwise to produce a deep purple-red solution. Dropwise addition of chloro(triethylphosphine)gold(I) (0.158 g, 0.451 mmol) in methylene chloride (2 mL) was performed. The resulting red-orange solution was left to stir for 2 h shielded from light. The addition of diethyl ether (30 mL) yielded an orange precipitate. The precipitate was isolated by filtration, washed with diethyl ether (3 × 20 mL), and dried in vacuo, affording **13** as an orange powder, 0.398 g (75%). ^{1}H NMR (500 MHz, CD_3CN, 25 °C): δ 8.052 (bs, 8 H), 7.829 (bs, 8 H), 7.3−7.6 (m, 24 H), 4.375 (t, J_{PH} = 4.2 Hz, 4 H), 0.693 (s, 18H). ^{31}P{H} NMR (202.5 MHz, CD_3CN, 25 °C): δ 27.834 (dd, J_{PP} = 34.6 Hz, J_{PP} = 34.6 Hz), 16.800 (ddd, J_{RhP} = 118.6 Hz, J_{PP} = 34.6 Hz, J_{PP} = 34.6 Hz). Anal. Calcd for $C_{60}H_{62}AuCl_2N_2P_4Rh$: C, 55.19; H, 4.79, N, 2.15. Found: C, 55.11; H, 4.65; N, 2.05.

5.4. Physical Methods. ^{1}H and ^{31}P{H} NMR spectra were recorded on solutions at 25 °C within the magnetic field of a Varian Mercury 300 or Inova 500 spectrometer, which was located in the Department of Chemistry Instrumentation Facility at the Massachusetts Institute of Technology. Chemical shifts are reported using the standard δ notation in ppm. ^{1}H NMR spectra were referenced to residual solvent peaks. ^{31}P NMR spectra were referenced to an external H_3PO_4 standard at 0 ppm.

X-ray diffraction experiments were performed on single crystals grown by diffusion of pentane into a concentrated tetrahydrofuran solution (**12**) or diethyl ether into a concentrated methylene chloride solution (**13**). Crystals were removed from the supernatant liquid and transferred onto a microscope slide coated with Paratone N oil. Selected crystals were affixed to a glass fiber in Paratone N oil and cooled to −173 °C (**12**) or −123 °C (**13**). Data collection was performed by shining Mo Kα (λ = 0.710 73 Å) radiation onto crystals mounted onto a Bruker CCD diffractometer. The data were processed and refined by using the program SAINT supplied by Siemens Industrial Automation, Inc. The structures were solved by direct methods (SHELXTL v6.10, Sheldrick, G. M., and Siemens Industrial Automation, Inc., 2000) in conjunction with standard difference Fourier techniques. All non-hydrogen atoms were refined anisotropically unless otherwise noted. Hydrogen atoms were placed in calculated positions. Details regarding the refined data and cell parameters are provided in the Supporting Information.

Acknowledgment. J.R. thanks the Fannie May and John Hertz Foundation for a predoctoral fellowship. J.D.S. acknowledges a postdoctoral fellowship from the National Institutes of Health. This work was supported by the National Science Foundation (Grant CHE-0450058).

Supporting Information Available: Atom numbering scheme, crystal data and structure refinement, atomic coordinates, bond lengths and angles, displacement parameters, and hydrogen coordinates for **12** and **13** and CIF data. This material is available free of charge via the Internet at http://pubs.acs.org.

IC0509276